

# Design and Performance Improvements in an A6 Relativistic Magnetron Using Particle-in-cell Code

Tusharika S Banerjee<sup>1,\*</sup>, Ayush Saxena<sup>2</sup>, Arti Hadap<sup>3</sup>, K. T. V. Reddy<sup>4</sup>, Apoorva Saxena<sup>5</sup>

<sup>1</sup>Department of Electronics and Telecommunication Engineering, Sardar Patel Institute of Technology, India

<sup>2</sup>Department of Electronics and Telecommunication Engineering, Ramrao Adik Institute of Technology (RAIT), India

<sup>3</sup>School of Technology Management & Engineering, Faculty of Physics, Mukesh Patel Vile Parle (W), India

<sup>4</sup>Pravara Educational Society's Pravara Technical Education Campus, Sir Visvesvaraya Institute of Technology (SVIT), India

<sup>5</sup>Department of Electrical Engineering, GLA University, India

Copyright©2019 by authors, all rights reserved. Authors agree that this article remains permanently open access under the terms of the Creative Commons Attribution License 4.0 International License

**Abstract** The aim of this paper is to suggest performance improvements in an A6 relativistic magnetron (RM) using the particle-in-cell (PIC), finite difference time domain (FDTD) simulation tool. It is shown that adding conductive strappings to the resonator assists in improving  $\pi$ -mode performance of the device by modulating the beam velocity profile. Comparisons have been made between the performance variables of a strapped and an unstrapped relativistic magnetron. In addition, the tapered mode converting structures are investigated which also assist in the  $\pi$ -mode performance of the RM. Also, a review is made on the basic operation of the RM with elements from both circuit and field theory.

**Keywords** Microwave Sources, Pulsed Power, Electron Devices, Electromagnetics

## 1. Introduction

The objective of this paper is to study and simulate relativistic magnetron (RM) which is a high-power microwave (HPM) generating source. Relativistic magnetron is a high-voltage, high-current and high energy (>500KeV) version of the conventional magnetron and has been regarded as one of the most efficient HPM source [1]. A Magnetron oscillator is a cross-field device which can generate microwaves in an approximate frequency range of 1-10 GHz. The conventional magnetrons operating at low voltages (<100kV) are capable of producing several megawatts of peak power. At relativistic voltages (400-1000 kV), a magnetron can generate high power microwaves in gigawatts range with efficiencies of 30% or less. **The comparison between the operating parameters of a conventional and a relativistic magnetron is presented in table 1 [1].** Relativistic

magnetron has been an increasingly popular device amongst researchers, especially for the reasons of its high-power capability, frequency tunability, and compactness amongst various HPM generating devices. The device under the scope of this paper is the MIT A6 relativistic magnetron [2][3][4]. The simulation work is carried out using the 'MAGIC3D' tools suite developed by ATK Mission Systems, USA. This tool is a Finite-Difference Time-Domain (FDTD) and Particle-In-Cell (PIC) based code, widely used for simulating processes which involve interactions between space charge and electromagnetic fields [5][6][7][8][15].

**Table 1.** Typical Operating Parameters for Conventional and Relativistic Magnetrons

Parameter	Conventional Magnetrons	Relativistic Magnetrons
Voltage	100kV	500kV
Current	~100A	5-10kA
Cathode Process	Thermionic and Secondary Emission	Explosive Emission
Pulse Duration	~1 $\mu$ sec	~100nsec
Rise Time	200kV/ $\mu$ sec	~100kV/nsec
Power	10MW	~1GW
Efficiency	~50%	~20-30%

In this paper, the theoretical modelling of the relativistic magnetron is discussed using elements from circuit and field theories. In order to understand the performance characteristics of the device, PIC simulations are performed for the following three cases: (a) Basic operation of MIT A6 relativistic magnetron using PIC code (b) Efficiency and mode characteristics improvement using a tapered horn antenna (c) Efficiency and mode characteristic improvement using strappings. These three cases are helpful in understanding the PIC modelling and design aspects of the MIT A6 relativistic magnetron.

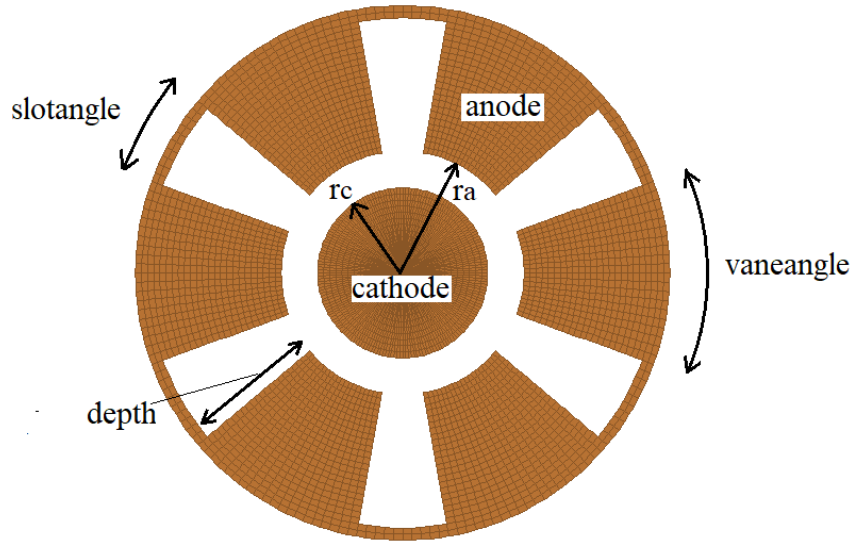


Figure 1(a). Schematic of the A6 RM resonator

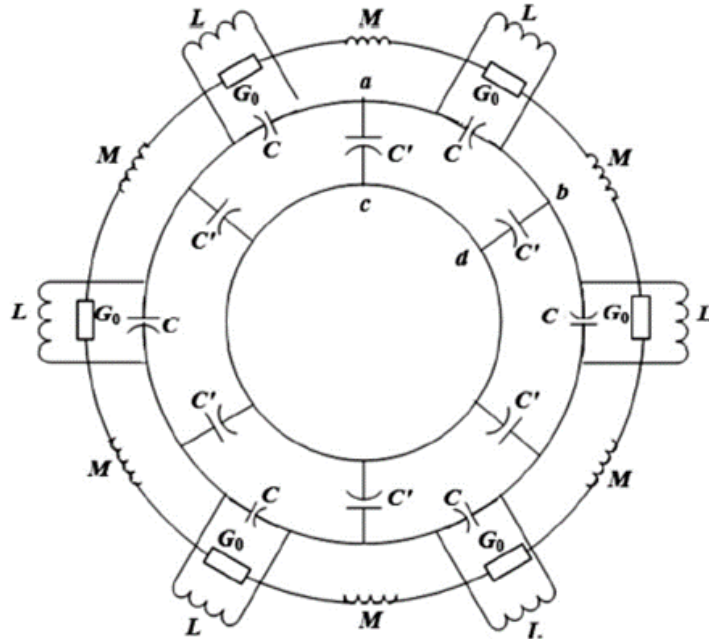


Figure 1(b). The equivalent circuit model of A6 RM [8]

## 2. Theoretical Background

The A6 relativistic magnetron consists of vanes and slots to form the slow wave structure (SWS), which makes the RF wave inside to resonate and grow. The fundamental mode frequency is determined by the capacitive and inductive values of the SWS [1]. For a six vane magnetron (\$N=6\$) there exists six operating modes (\$n=1,2,\dots,6\$), with \$N/2\$ being the \$\pi\$ mode and \$n=6\$, the \$2\pi\$ mode.

Theoretical formula for \$\pi\$ mode frequency is usually obtained by two approaches. First is the equivalent circuit method which derives resonant frequency as a function of structure dimensions [8]. The schematic of an A6 RM

cross-section is shown in Fig. 1(a) and its equivalent circuit model is shown in Fig. 1(b), where \$C\$, \$G\_0\$ and \$L\$ are the equivalent capacitance, the equivalent conductance and the equivalent inductance, respectively.

$$\omega_m = \frac{\omega_0}{\omega_1} \tag{1}$$

where,

$$N = 6, \quad K = \sqrt{\pi^2 - \frac{8 \times (r_i - r_c)}{r_i}}, \quad m = \text{mode number}$$

$$\omega_0 = \frac{\left( 2 \cdot r_0 \cdot \ln\left(\frac{r_0}{r_i}\right) + \frac{\theta_s \cdot \theta_v \cdot d}{\tan\left(\frac{\theta_s}{2} + \frac{\theta_v}{2}\right) \cdot (\pi - \theta_s - \theta_v)} - 2 \cdot d \right)^{-\frac{1}{2}}}{\left( \frac{\mu_0 \times \epsilon_0}{6} \cdot (2 \cdot r_0 + r_i) \cdot \left( 1 - \left(\frac{d}{l}\right)^2 \right) \right)^{\frac{1}{2}}}$$

and

$$\omega_1 = \left( 1 + \frac{\frac{\theta_v}{\ln\left(\frac{r_i}{r_c}\right)} + \left(\frac{2 \cdot r_c}{r_i \cdot K}\right) \cdot \left( \ln\left(\frac{\pi + K}{\pi - K}\right) - \ln\left(\frac{2 \cdot \theta_s + \pi + K}{2 \cdot \theta_s + \pi - K}\right) \right)}{2 \cdot \left( 1 - \cos\left(\frac{2 \cdot m \cdot \pi}{N}\right) \right) \cdot \left( \frac{2 \cdot r_0}{\theta_s \cdot d} \cdot \ln\left(\frac{r_0}{r_i}\right) + \frac{\theta_v}{\tan\left(\frac{\theta_s}{2} + \frac{\theta_v}{2}\right) \cdot (\pi - \theta_s - \theta_v)} - \frac{2}{\theta_s} \right)} \right)^{\frac{1}{2}}$$

The resonant frequency (Hz) is given by,

$$freqR = \frac{\omega_m}{2\pi} \quad (2)$$

The equivalent circuit model shown in Fig. 1(b) can be used to find out the resonant frequency for the magnetron. Given the physical dimensions of the device, the resonant frequencies for various operating modes can be obtained from eq. 1 and eq. 2.

**Table 2.** Dimensions of MIT A6 RM

Outer radius of anode ( $r_o=r_a+depth$ )	4.11 cm
Anode radius( $r_a$ )	2.11 cm
Cathode radius( $r_c$ )	1.58 cm
Resonator length( $L$ )	7.2 cm
Vane angle ( $\theta_v$ )	40 deg
Slot angle ( $\theta_s$ )	20 deg

Considering the standard MIT A6 device dimensions shown in table 2, the relationship obtained between the resonant frequency and the mode number is represented by the curve shown in Fig. 2. Notice the resonant frequency for degenerate mode pairs 1 & 5 and 2 & 4, which have the same resonant frequency. For a six-vane magnetron, mode 3 (or N/2) is called the  $\pi$  mode. In this case, the  $\pi$  mode

frequency is approximately 2.45 GHz. The  $2\pi$  mode frequency is nearly twice to that of the  $\pi$  mode frequency. An alternate field theoretical approach to calculate the resonant frequency of a RM is based on equivalence of admittance ( $Y_n = -Y_r$ ) in the resonator vanes ( $Y_n$ ) and AK cylindrical gap region ( $Y_r$ ), given as [9],

$$Y_n = j \sqrt{\frac{\epsilon_0}{\mu_0}} \frac{Nh}{2\pi r_a} \sum_{m=-\infty}^{\infty} \left( \frac{\sin \gamma \theta}{\gamma \theta} \right)^2 \cdot \frac{Z_\gamma(kr_a)}{Z_\gamma'(kr_a)} \quad (3)$$

$$Y_r = j \sqrt{\frac{\epsilon_0}{\mu_0}} \frac{h}{\psi a} \frac{J_0(ka)N_1(kb) - J_1(kb)N_0(ka)}{J_1(ka)N_1(kb) - J_1(kb)N_1(ka)} \quad (4)$$

The solution for resonant frequency involves finding out of intersection points after superimposing the  $Y_n$  and  $-Y_r$  curves. The MIT A6 dimensions given in table 2 are used to obtain admittance curves shown in Fig. 3. The points A, B and C points shown in Fig. 3 can be used to obtain resonant frequency for various modes of magnetron operation [10]. The values on the horizontal axis (x), corresponding to the points A, B and C are related to the device dimensions as well as the wave number, hence, with the resonant frequency of the respective mode as shown in eq. 5.

$$x \approx \frac{2}{(r_a + r_c)} \approx \frac{k}{100} \approx \frac{2\pi}{\lambda} \quad (5)$$

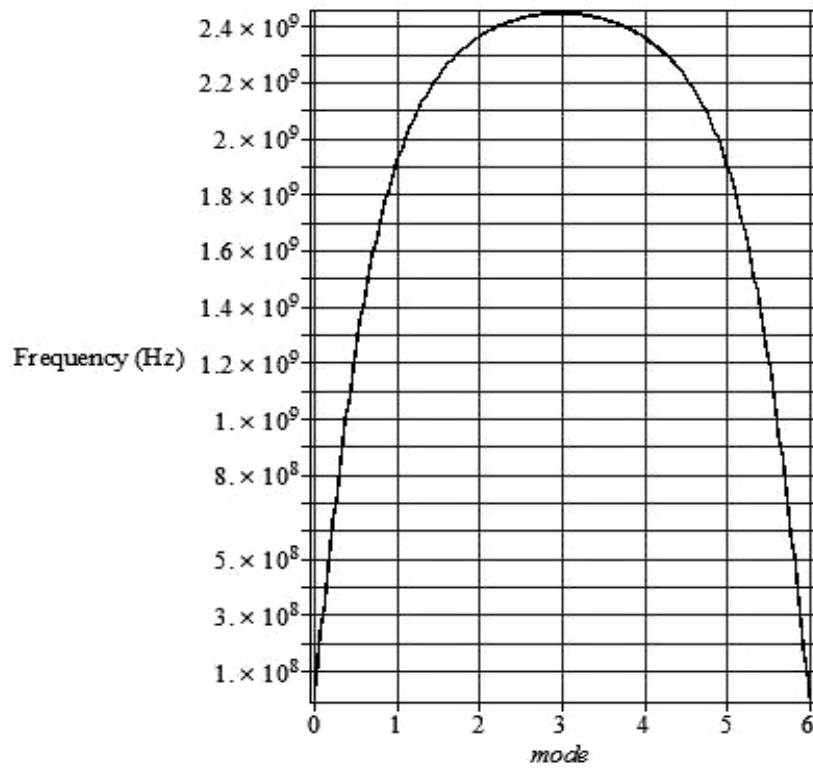


Figure 2. Resonant Frequency vs mode number

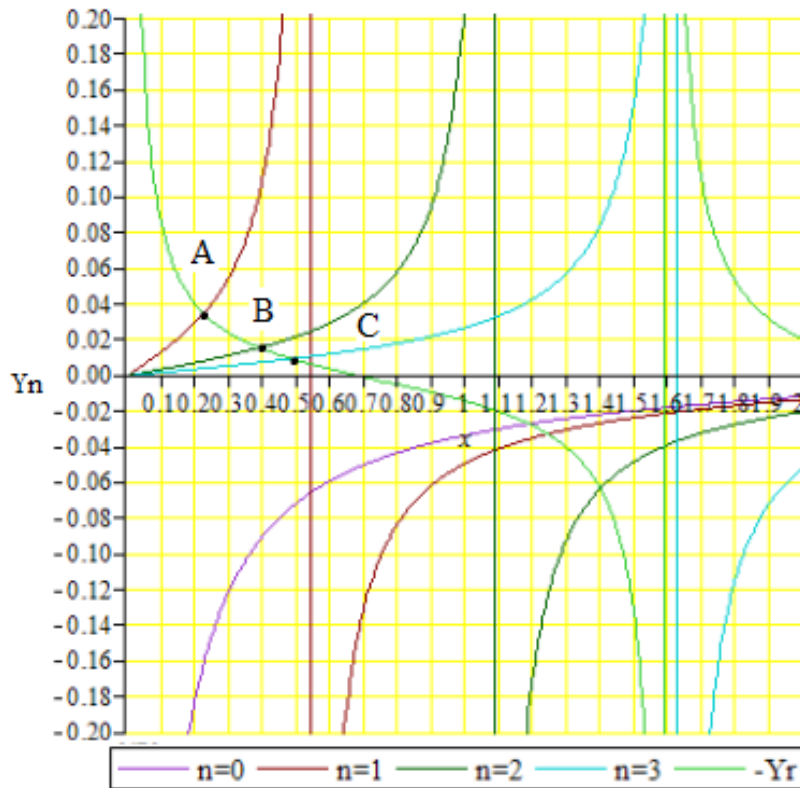


Figure 3. Equivalence of Admittance

In the following section, PIC simulations are used to model and analyze the performance characteristics of the MIT A6 relativistic magnetron. In Case 1, the basic operation of a relativistic magnetron is shown followed by Case 2 and Case 3 which demonstrate more complex configurations in order to understand performance and design aspects of the RM.

### 3. Simulation Environment and Results

The RM is investigated using the PIC tool suite with the help of three different cases. The combination of the given examples highlights different aspects of the design.

#### 3.1. Case 1: Basic Operation of 6 Vane RM

The structure of an A6 relativistic magnetron consists of six cavities with an azimuthal spacing of 60 degrees. The radius of cathode ( $r_c$ ) and radius of anode ( $r_a$ ) are taken as 1 cm and 2.08 cm, respectively. The anode-cathode (AK) gap is 1.08cm, resonator vane depth is 2.075 cm and the length of the resonator in  $z$  direction is 7.2cm. These dimensions are slightly different from MIT A6 so as to fit the mesh grid size. The cross-sectional schematic of the three-dimensional model of A6 relativistic magnetron is shown in Fig. 4(a). The operating voltage is set to 300 kV and the applied magnetic field strength is 0.25T, which is in accordance with the operating region from the  $V$ - $B_z$  curves for Hull and Bunemann-Hartree conditions for the  $\pi$  mode operation.

The radiated output power calculated at one of the vanes is shown in Fig. 4(b) and its corresponding FFT is shown

in Fig. 4(c), illustrating the presence of a dominant  $\pi$  mode. The average value of the instantaneous power collected on the anode bore after using a step filter period of 1ns is around 80MW. This filtering provides a temporal averaging that reduces the statistical noise associated with particles. The effect of step filtering is further illustrated in section 3.3. The average value of the emitted current from cathode is around 4.7kA. Particle phase space at 35.7 ns is shown in Fig. 4(d). Formation of three spokes can be observed. The dominating  $\pi$  mode frequency observed is 2.36GHz.

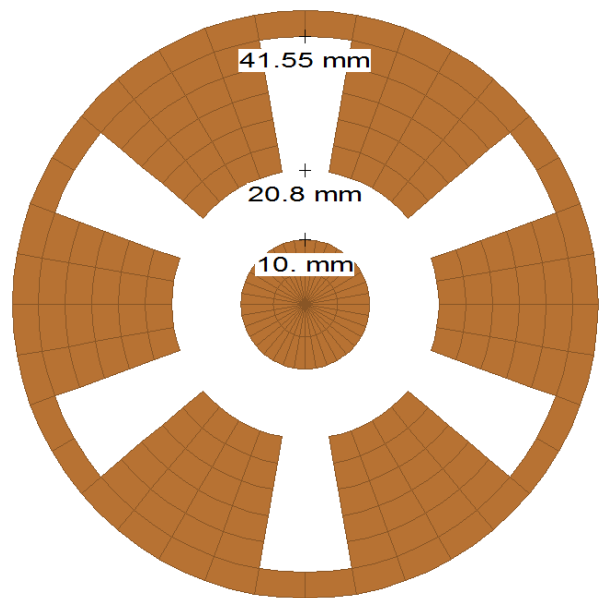


Figure 4(a). Magnetron Cross-section with dimensions

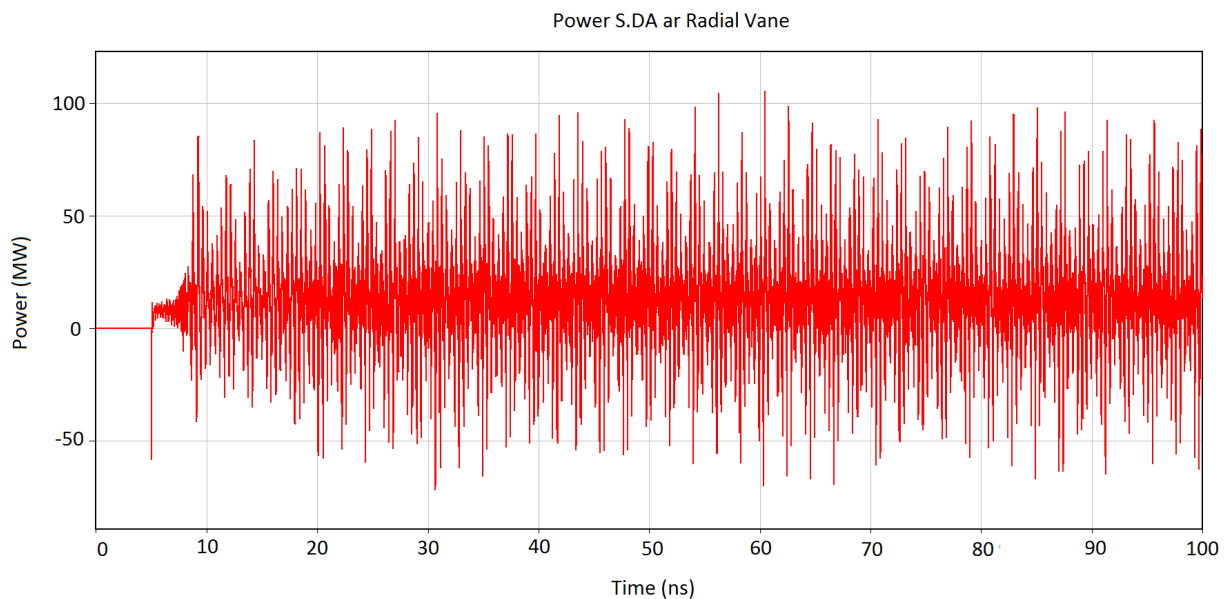


Figure 4(b). Radiated Power Output

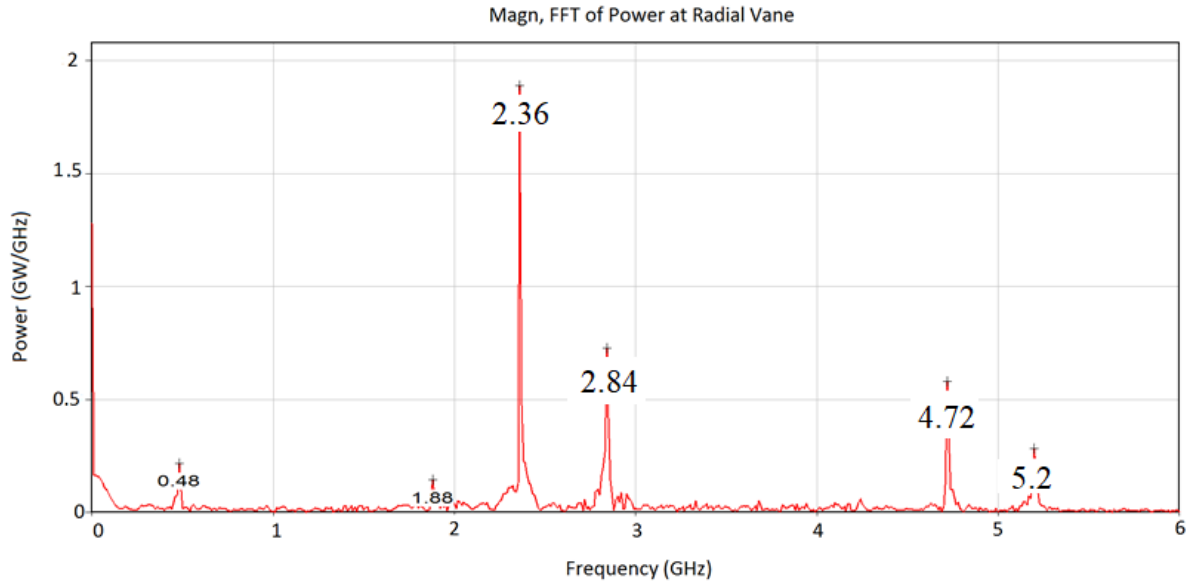


Figure 4(c). FFT of the radiated power

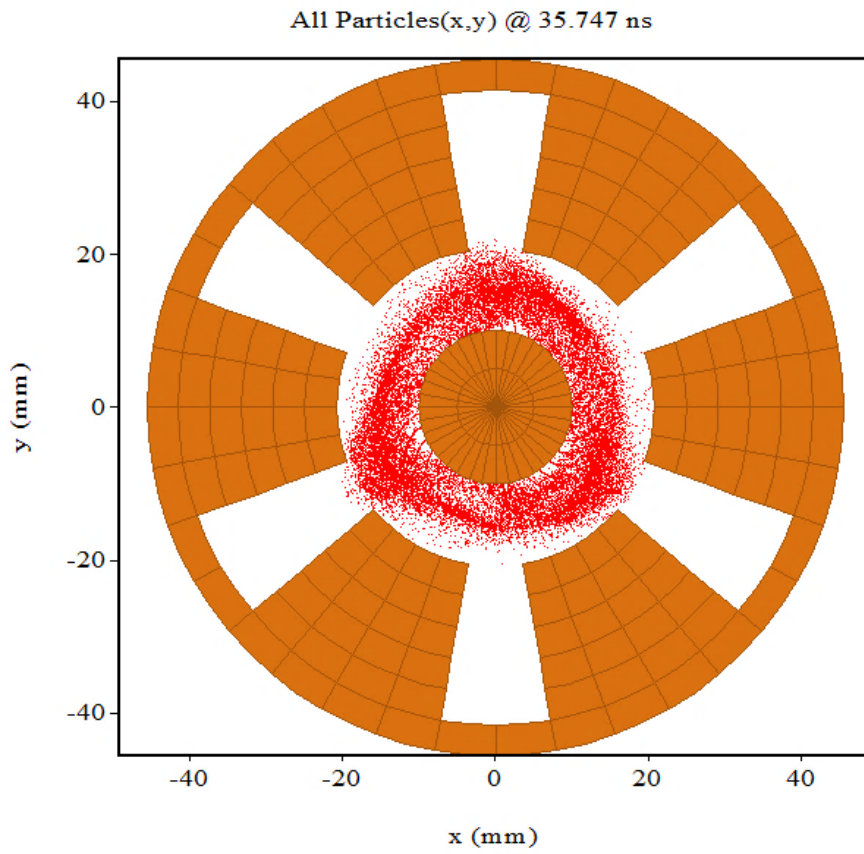


Figure 4(d). Particle phase space at 35.747 ns

The generated microwave power in relativistic magnetrons is extracted radially through single or multiple iris of different width. In [11], it has been shown that in general, output power and efficiency increase approximately linearly with increasing iris width until the total Q becomes too low. Beyond this point, mode competition or switching occurs and efficiency decreases. There are various methods employed to improve the microwave power efficiency and the peak radiated power. In [3][4], method of axial power extraction with  $\pi$  as dominant mode of operation is used to improve the performance characteristics of the device. Most often, only the  $\pi$  mode frequency lies in the S-band (2-4 GHz) as the  $2\pi$  mode frequency is nearly twice that of the  $\pi$  mode, hence, for S-band operation it is desirable to operate in the  $\pi$  mode. The A6 magnetron operation having resonator vanes partially loaded with low loss dielectric material [12][13] has been reported performing in  $2\pi$  mode with high radial output power and low start up time in comparison to the unfilled side resonators. A modified

configuration of relativistic magnetron with axial power output or diffraction output has been proposed in [14] and 3D particle-in-cell simulations using simulation-code MAGIC3D were carried out to demonstrate the effectiveness of the modified configuration.

### 3.2. Case 2: Relativistic Magnetron Coupled with Horn Structure

In [3], a RM is coupled with a tapered waveguide configuration and significant efficiency improvement have been reported, from 3% to 37%. Case 2 studies the effect of a coupled tapered waveguide structure or a horn antenna coupled with the relativistic magnetron for the axially radiated microwave output as shown in Fig. 5(a). The diffraction output has been observed using two types of horn structures [3]. The dimensions of the resonator and operating parameters of the magnetron are shown in table 3.

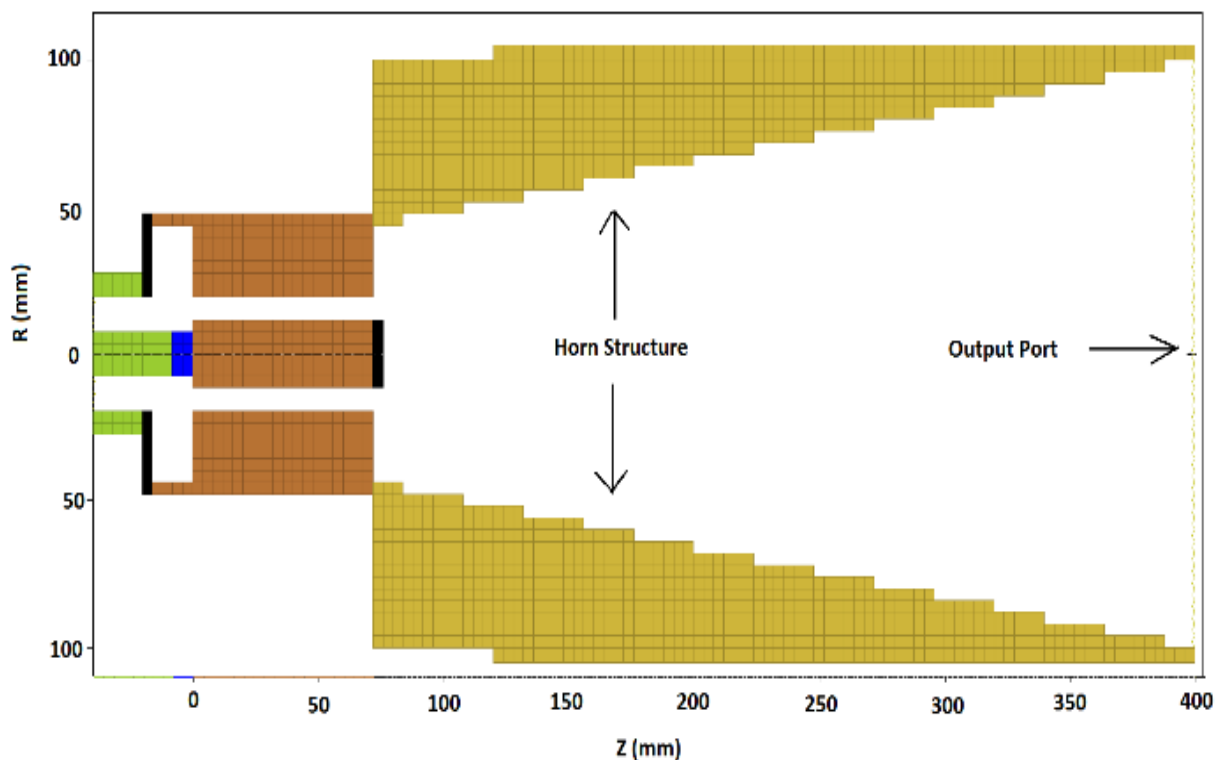


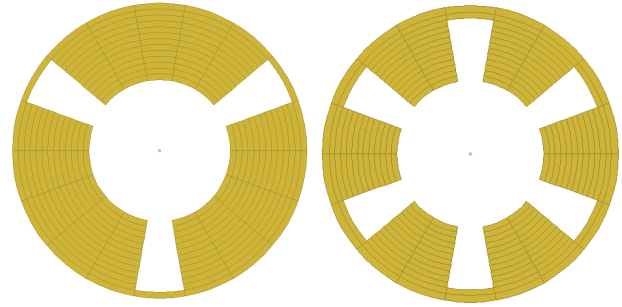
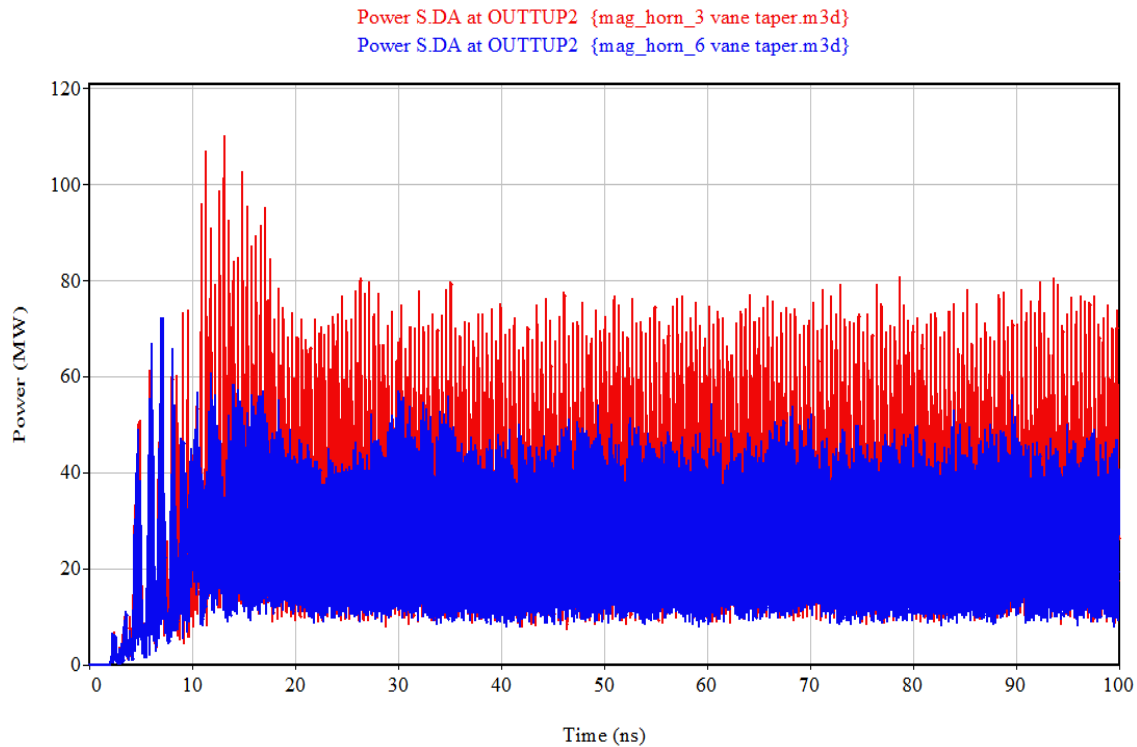
Figure 5(a). Schematic of the Magnetron with Horn antenna

**Table 3.** DEVICE Dimensions

Parameter	Values
Cathode Radius	1.2 cm
Anode Radius	2 cm
A-K Gap	0.8 cm
Vane Depth	2 cm
Operating Voltage	400 kV
Magnetic Field (B)	0.58 T
Horn Angle	~17 deg

The horn structure is tapered from inside in two different ways. In one configuration only three vanes are tapered and in other configuration all six vanes have been tapered Fig. 5(b). The output microwave power and the microwave efficiency are affected by the configuration of the tapered mode converter. The comparison between the microwave power obtained at the output port and the corresponding frequency components for the 3-vane and 6-vane horn configurations can be observed in Fig. 5(c), (d) and (e). The red and blue curves correspond to 3-vane and 6-vane horn

configurations, respectively. The configuration with 3-vane assist in generation of  $\pi$  mode frequency with higher power (peak power ~80MW) being observed at the output port (Fig. 5(c)). The output power obtained at the horn boundary has both  $\pi$  and  $2\pi$  mode frequency components (Fig. 5(d)). On the contrary, the six-vane tapered configuration has only  $2\pi$  mode frequency component with lower power (peak power ~55MW) obtained at the output port. The average value of the current collected at anode bore is ~9kA.

**Figure 5(b).** Three and six tapered vanes<sup>[3]</sup>**Figure 5(c).** Comparison of radiated power at horn boundary

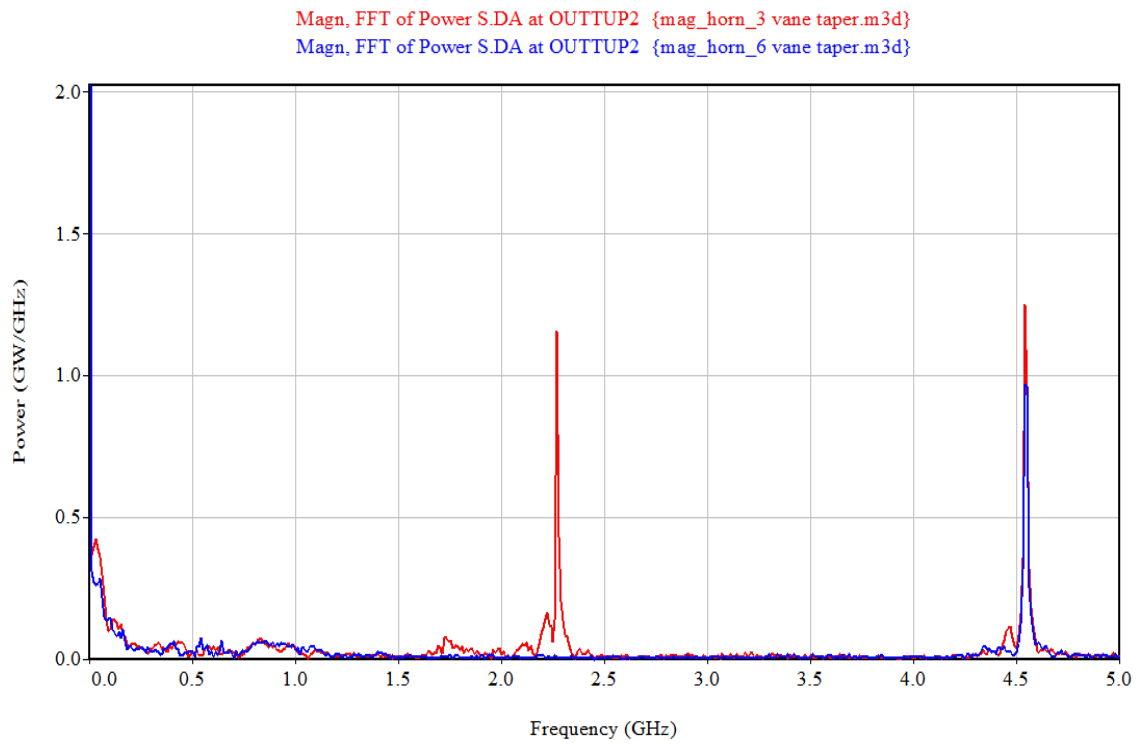


**Figure 5(d).** Comparison of Mag, FFT of Radiated power

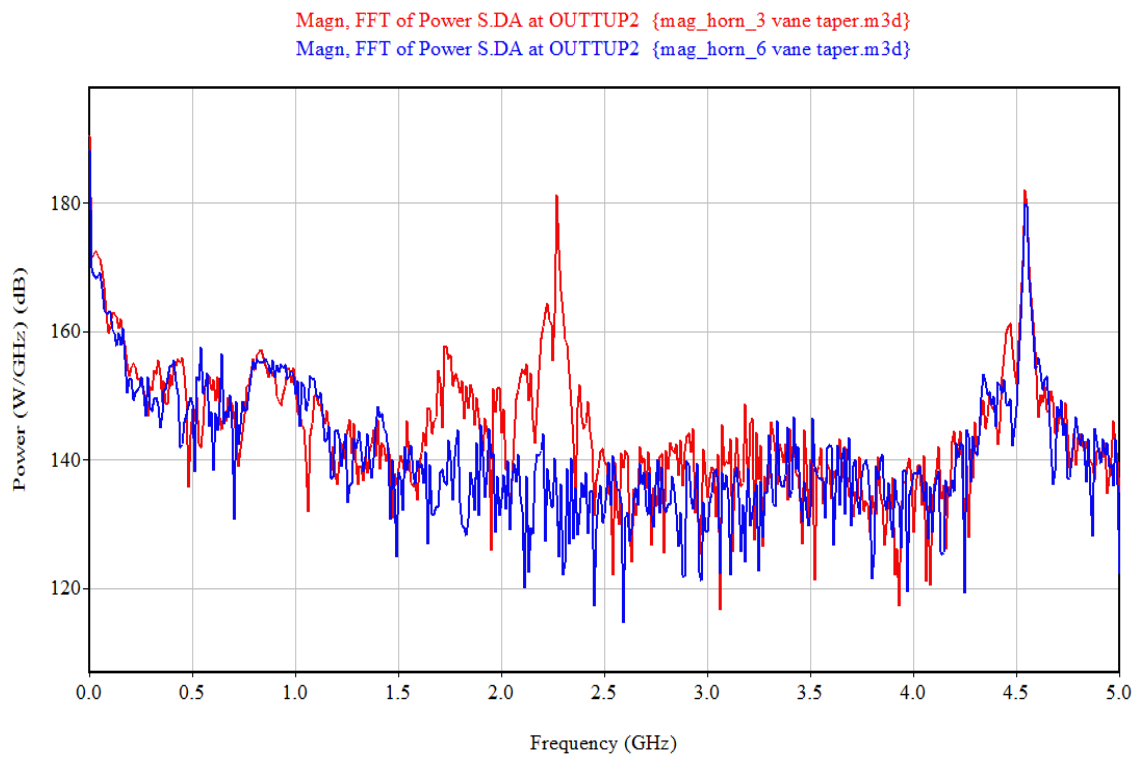


**Figure 5(e).** Comparison of Mag, FFT of Radiated power (in dB)

### 3.3. Case 3: Relativistic Magnetron with Strappings

In [15], it is shown that introduction of dielectric side-wall in the magnetron resonator assist in  $\pi$  mode formation. It has been shown in this section that introduction of conductive strappings or shorting of alternate anode resonant cavities result in further improvement in stable  $\pi$ -mode operation. The relativistic magnetron simulated here uses dimensions from table 3 and cylindrical coordinates ( $r$ ,  $\phi$  and  $z$  coordinates) are

used to model the same. The  $\sim 300\text{kV}$  input voltage pulse is shown in Fig. 6(a) with a step filter period of  $1\text{ns}$ . The same has been represented in Fig. 6(b) with a step filter of  $5\text{ns}$ . Both Fig. 6(a) and 6(b) are similar to each other (the purpose of this postprocessing filter is to remove statistical noise) and hence the choice of the filter period will be partly based upon the extent of noise in the signal. ‘Step’ filtering is more effective on signals with known periodic behavior. The value should be an integer number of periods to get a smooth average over the periodic phenomenon.

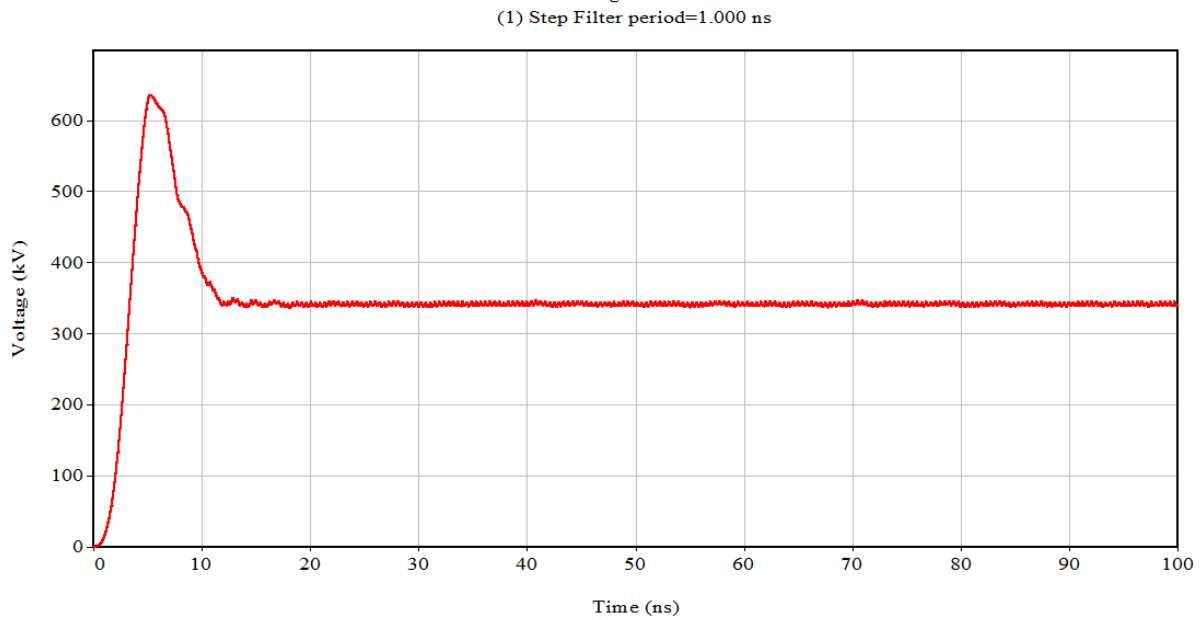


Figure 6(a). Input Voltage Pulse with 1ns step filter

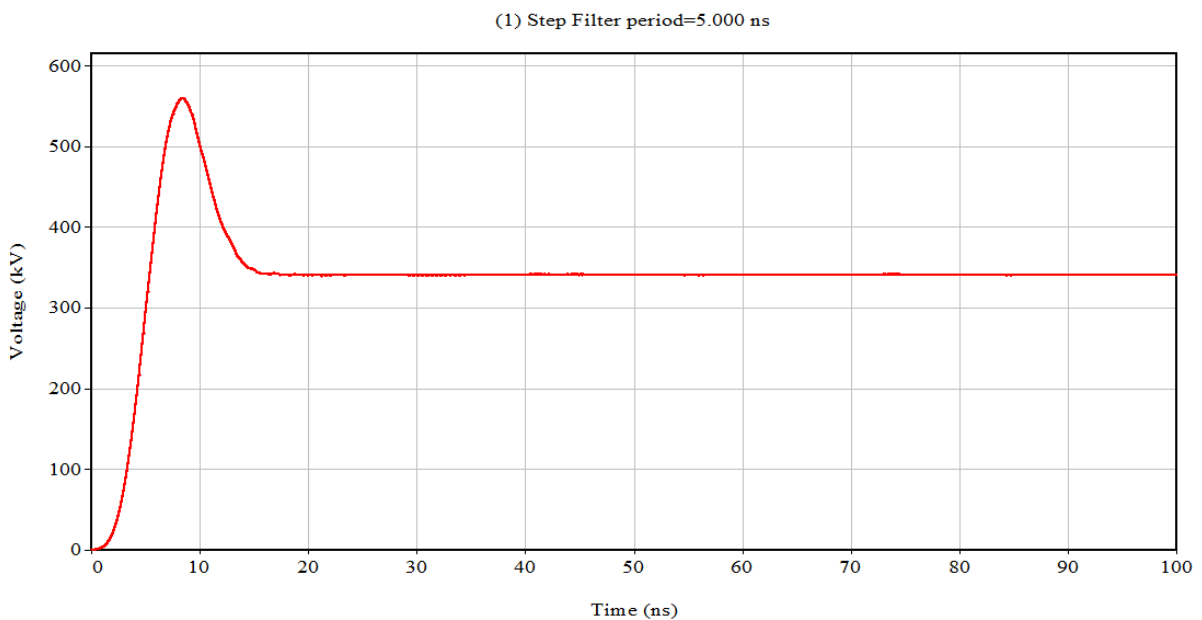


Figure 6(b). Input Voltage Pulse with 5ns step filter

Fig. 7(a) and 7(b) show the conductive strapping (in orange) which are introduced to short the alternate anode resonator cavities. Fig. 7(b) and 7(c) also show the particle phase space ( $r$ - $z$  plane) or position of electrons in the beam originating from cathode at  $\sim 11$  ns time instant. Formation of three spokes denote the formation of  $\pi$  mode. Fig. 7(d)

shows the comparison of power and frequency output between two magnetron configurations, one with strappings (shown in red) and one without strappings (shown in blue). It is observed that the radiated microwave power is more when strappings are used.

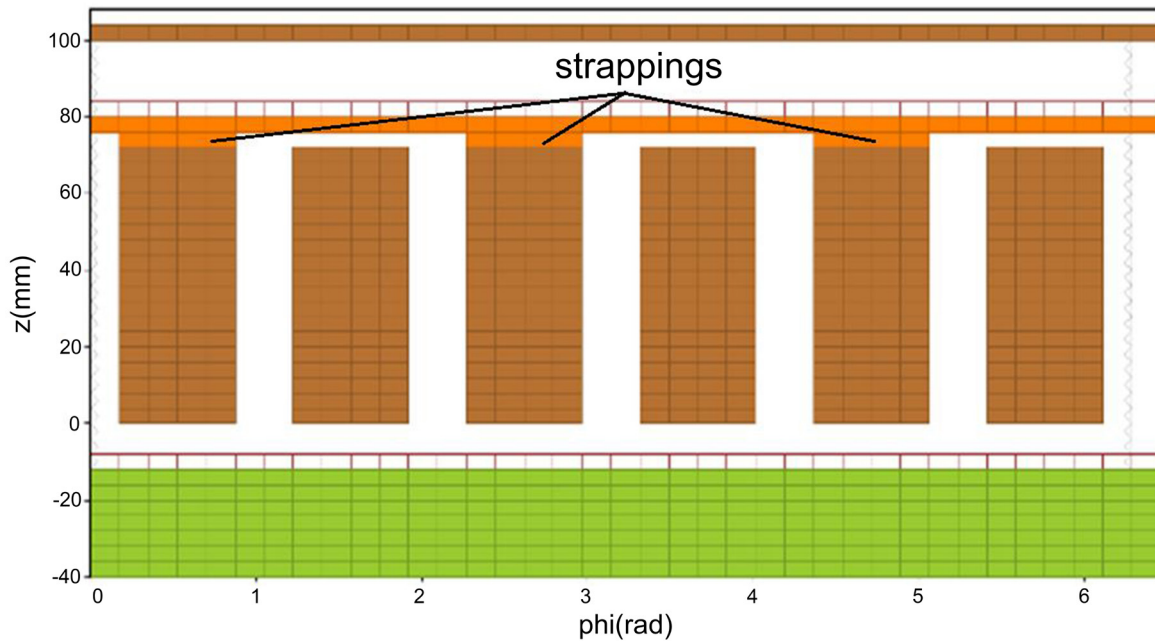


Figure 7(a). Strapping to short alternating vanes ( $z$  vs  $\phi$  plane)

All Particles( $z,r$ ) @ 11.990 ns

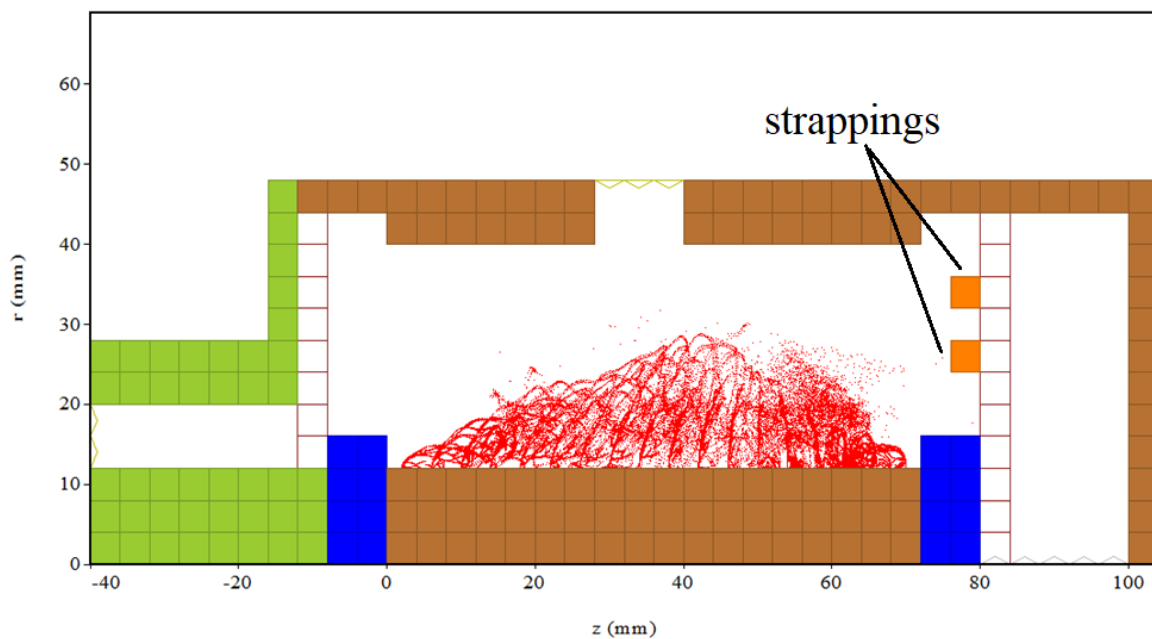
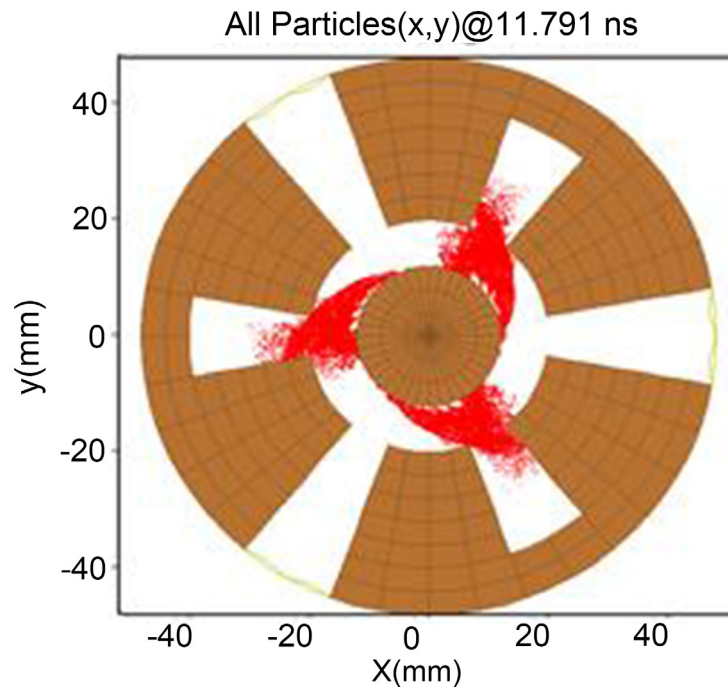
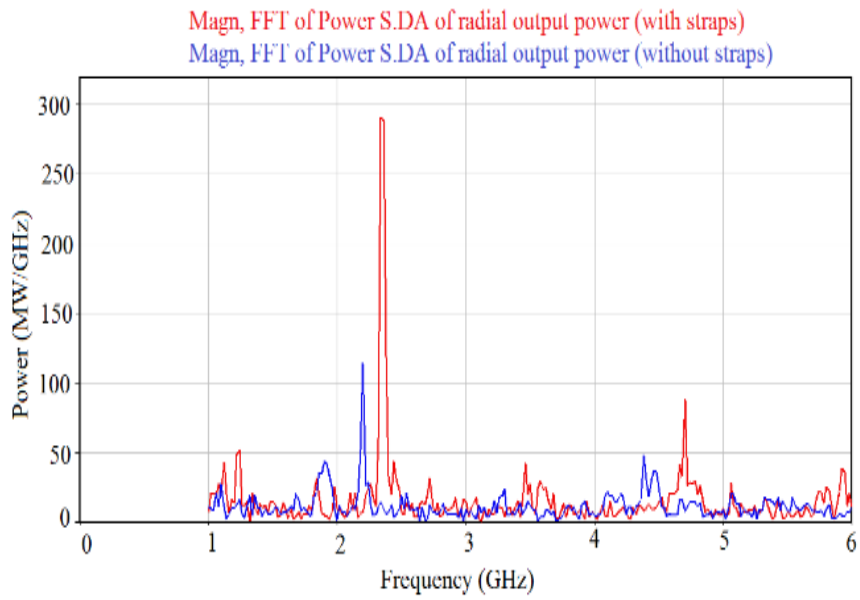


Figure 7(b). Strapping to short alternating vanes ( $r$  vs  $z$  plane)



**Figure 7(c).** Formation of three spokes (r vs phi plane)



**Figure 7(d).** Comparative plot showing dominant frequency and radiated output power

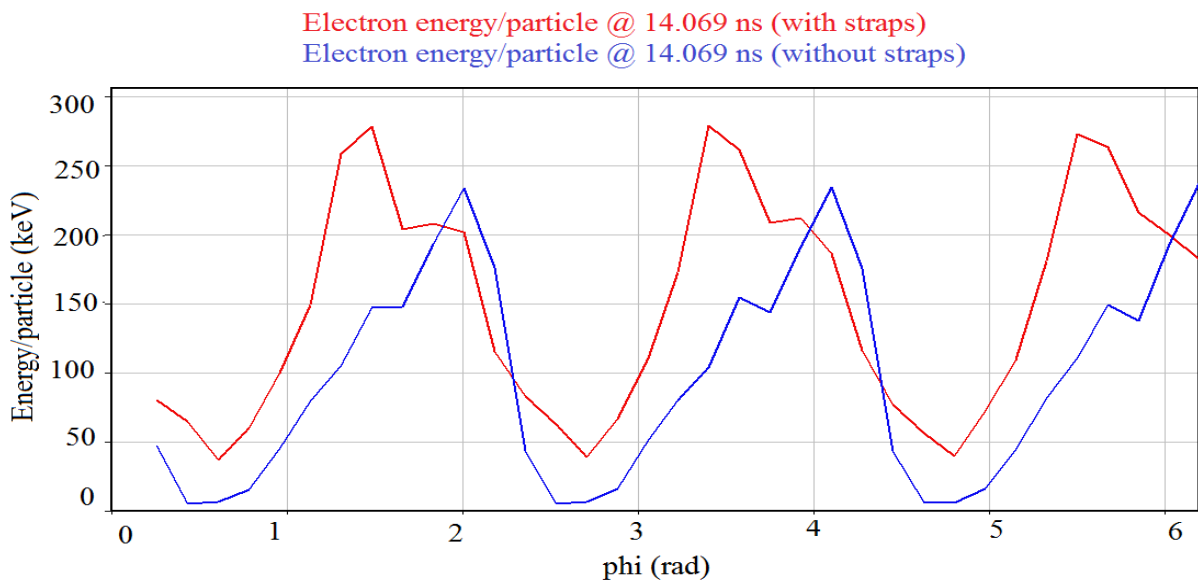


**Figure 7(e).** Comparison of average kinetic energy per particle for electrons rotating inside the resonant cavity

This can be attributed to improved  $\pi$  mode performance of the device. Also, the average particle energy comparisons are shown in Fig. 7(e) at  $\sim 14$  ns. Here, it is observed that the average kinetic energy of particles or the electron beam in general is more for the strapped magnetron. Hence, it has been found that introduction of strappings aid in reducing mode competition and improving performance characteristics of the device.

## 4. Conclusions

The classical theoretical formulations have been studied for the MIT A6 relativistic magnetron. PIC three-dimensional simulations are used to model the device and understand the performance characteristics. The RM coupled with a horn 3-vane tapered structure is found to assist in  $\pi$  mode operation of the device, which is the desired mode of operation for maximum efficiency. Introduction of strappings in the magnetron resonator are also found to assist in the  $\pi$  mode operation, hence, improvement in microwave peak power and efficiency is observed. Additional comments have been made on the energy of the particles involved. Further analysis of the beam and plasma dynamics can provide better understanding of the device's operation.

## Acknowledgements

The authors of the paper would like to acknowledge Pillai College of Engineering, New-Panvel for its constant support and encouragement. The authors would also like to thank Dr. Navdeep M. Singh, Professor, Veermata Jijabai Technological Institute, Mumbai for supporting this work.

## REFERENCES

- [1] J. Benford, J. Swegle, and E. Schamiloglu, *High Power Microwaves*, 2nd ed. New York: Taylor & Francis, 2007.
- [2] H. Sze, B. Harteneck, J. Benford and T. S. T. Young, Operating Characteristics of a Relativistic Magnetron with a Washer Cathode, in *IEEE Transactions on Plasma Science*, vol. 15, no. 3, pp. 327-334, June 1987.
- [3] M. I. Fuks and E. Schamiloglu, 70% efficient relativistic magnetron with axial extraction of radiation through a horn antenna, *IEEE Trans. Plas.Sci.* Vol.38, no. 6, pp1302-1312, 2010.
- [4] Wei Li, Yong-gui, Liu Ting Shu, Han-wu Yang, Yu-wei Fan, Cheng-wei Yuan and Jun Zhang, Experimental demonstration of a compact high efficient relativistic magnetron with directly axial radiation, *Physics of plasmas* 19,013105, 2012.
- [5] C.K. Birdsall, *IEEE Trans. on Plasma Science*, Vol. 19, No. 2, April 1991, pp. 65-85.
- [6] C.K. Birdsall, and A.B. Langdon, *Plasma Physics via computer simulation*, IOP Publishing, 1991.
- [7] L. Ludeking, A. Woods, L. Cavey, *Magic User Manual 3.2*, Alliant Techsystems, U.S.A, 2011.
- [8] A. Saxena, A. Roy, K. Kanakgiri, S. Petkar, F.S. Kazi and N.M. Singh, "Particle-in-cell modeling of axial and coaxial virtual cathode oscillators", *IEEE Transactions on Plasma Science*, July 2016.
- [9] Y Fan, J Liu, H Zhong, T Shu, and Z Li, Theoretical investigation of the fundamental mode frequency of A6 magnetron, *J.Appl. Phys.* 105, 083310, 2009.
- [10] G. B. Collins, *Microwave Magnetrons*, McGraw-Hill Book

Company, Inc., 1948.

- [11] Raymond W. Lemke, T. C. Genoni, and Thomas A. Spencer, Effects that Limit Efficiency in Relativistic Magnetrons, *IEEE Trans. on plas.sci.vol.28*, no.3, 2000.
- [12] S.H.A Hashemi, Dielectric cavity relativistic magnetron, *Appl. Phys. Lett.*, Vol.96, no.8, pp. 081503-1-081503-3, 2010.
- [13] Shivendra Maurya, V. V. P. Singh, and P.K.Jain, Study of output performance of partially dielectric loaded A6 relativistic magnetron, *IEEE Trans. on plas.sci.vol.40*, no. 4, 2012.
- [14] M. Daimon and W. Jiang, Modified configuration of relativistic magnetron with diffraction output for efficiency improvement, *Appl. Phys.Lett.* 91, 191503, 2007.
- [15] A. Saxena, R. Barakade, N. M. Singh and A. Patel, Comparative analysis of radial and axial power output in relativistic magnetron and effect of dielectric side-walls introduced in the resonator on dominant operating mode, *EuMA, Cambridge Univ. Press, International Journal of Microwave and Wireless Technologies*, 6(6), pp. 645–651, 2014.